# The Dynamo Process in Pulsar Magnetosphere and Radio Emission of Pulsars

Bi-Ping Gong*

The pulsar radio emission mechanism remains an enigma since over half a century. A radiation process requires not only to explain the coherency and high degree of polarization of the emission, but also nanobursts, characteristic frequency of emission, and problems like "death line", which cannot be well understood in the context of long standing cap models and recent models of magnetic reconnection. This article proposes a dynamo process in pulsar magnetosphere. Through centrifugal force the last closed magnetic field lines can be amplified to a critical value of, $B_T \sim 10^4$T, which triggers magnetic reconnection responsible for the instability required in coherent curvature radiation, so that a number of problems can be interpreted. The time scale of magnetic field pile up and relaxation can be short or long for young or old pulsars respectively, which naturally account for the diverse intermittencies exhibited in pulsars and FRBs.



## I. INTRODUCTION

The bright radio pulse requires a coherent emission of in phased charges accelerated by the pulsar, so that $N$ charges radiating $N^2$ times the power in spontaneous emission per single charge.

There are two major coherence mechanisms, maser and antenna mechanisms[1–4], which adopt a secondary pair plasma and place the origin of the pulsar radiation in the inner region of the magnetosphere. The antenna mechanism involves a bunch of particles with enhanced the power emitted spontaneously; and maser mechanism requires a negative absorption.

However, they all require a certain kind of plasma instability. Whereas, no mechanism exists that is fast enough to create the bunches and to maintain their shape for sufficiently long times [5]; despite coherent curvature emission (CCE) being a widely favoured as the pulsar radio emission mechanism.

On the other hand, the global solution for force free magnetospheres was obtained using various numerical techniques [6–9], assuming that the only surviving component of electric field is that perpendicular to the magnetic field[10].

Although remarkable progress have been made in recent years, on simulations of magnetospheric current sheet and reconnection responsible for coherent emission mechanism, i.e., radio emission from the Crab and other pulsars with high magnetic field at the light cylinder [11–14]. However, one cannot regard such solutions as completely realistic, since various artificial procedures are required to keep the codes, which affect strongly the behavior of the equatorial current sheet, and subsequent dissipation through magnetic reconnection[9].

On the other hand, the force free solution actually corresponds to the state of minimum global magnetic energy, which can be obtained by minimizing the global magnetic energy $W = \int_V B^2 dV$ while keeping the global magnetic helicity, $H = \int_V \mathbf{A}\cdot\mathbf{BdV}$ constant[15]. In Taylor's conjecture, the magnetic field configuration formed as the end-state of a turbulent relaxation process is one for which the magnetic energy is minimized with the radial profile of parallel current tends to flatten[16].

In other words, dissipation process such as pair production, plasma acceleration and radiation are more likely exhibited in the dynamo process under the tension between the global helicity density and local dissipation, rather than the state of minimum energy.

There are some common challenges to both models of CCE at polar gap and radiation from reconnection at outer magnetosphere, i.e., pulsar radiation in over 5 orders of magnitude in rotation period and 6 orders of magnitude in magnetic field, producing more or less similar emission characteristics, over a very broad-band emission from $\sim$ 10MHz-100 GHz. In particular, the discovery of a highly magnetized, 75.88 s period, radio-emitting neutron star, PSR J0901-4046, located beyond the "death line" as defined by[2, 17], challenges the polar cap models demanding a sufficient electric field parallel to magnetic field; and also the reconnection induced radiation requiring strong light cylinder magnetic field [18].

Furthermore, recent observations show that a pulse profile actually built up a large number of localized, transient events, which are described as: intermittency, fine structures, discrete emissions, short-lived emission centers, microstructure and nanoshots[19]. Such microstructure is too rapid to be caused by propagation through turbulence in the Crab nebula or in the interstellar medium[20], which becomes more severe in the case of nanobursts[21]. Those bright nanobursts must be coherent, radiating in characteristic emission frequency, and then passing through a highly transparent medium to avoid being thermalized[22]. Those microstructure and characteristic frequency may provide clue to the origin of CCE.

This paper suggests a dynamo process occurring in pulsar magnetosphere, the resultant reconnection near light cylinder naturally provides seed of instability expected by CCE. The arrangement is as follows.

In Section (II) the pulsar spin gives rise centrifugal force driving plasma of closed field lines toward the light

* Also at Department of Physics, Huazhong University of Science and Technology

cylinder radius. As a result, the equatorial branch of the Y-shaped current layer becomes so compressed that that a rapid magnetic reconnection is triggered through chain of plasmoids, which leads to pair production and Alfven wave (AW). In Section (III), the ejected relativistic particles in phase with AW drift along magnetic field of open field lines giving rise to coherent curvature emission responsible for observation. Section (IV) discusses circuit closure and the origin of orthogonal polarization mode (OPM). Section (V) applies the dynamo model to various sources, typical pulsars, Rotating Radio Transients (RRATs) and Fast Radio Bursts (FRBs).

## II. THE CRITERIA OF MAGNETIC FIELD AND RECONNECTION

The interaction of global helicity density and local dissipation of the pulsar magnetosphere resembles that of the solar dynamo, which can be simplified into two regeneration mechanisms. Firstly, differential rotation stretches out an initially poloidal field generating a toroidal component (the $\omega$-effect); and secondly the "rise and twist" motion of cyclonic convection generates small-scale meridional loops from an initially toroidal field (the $\alpha$-effect).

Such an oscillation between toroidal and poloidal field can be simplified by a poloidal field of rotational symmetry, under a differential rotation, $\omega(r,\theta)=\omega(r^0,\theta^0)$, drawing out the lines of force along circles of latitude and thus producing a toroidal field [23],

$$B_\phi=(\partial\phi/\partial r^0)B_r+(\partial\phi/r^0\partial\theta^0)B_\theta \tag{1}$$

Ignoring the radial component at right hand side of Equation (1), it can be further simplified,

$$B_\phi\approx\frac{\partial\phi}{r^0\partial\theta^0}B_\theta=\frac{\partial\phi}{\partial t}\frac{\partial t}{r^0\partial\theta^0}B_\theta\approx\dot{\phi}\partial t\frac{B_{lc}}{\delta}\approx\dot{\phi}t\frac{B_{lc}}{\delta}$$

where $r^0\partial\theta^0\approx\delta$ can represent the thickness of the apex of the last closed field line near the light cylinder as shown in Fig1a. The deformation of field line can be described by a rotation angle, $\phi=\dot{\phi}t$, which indicates an increase of toroidal field by $t^2$[23].

Such a dynamo amplification of magnetic energy inevitably reaches a point where the plasma flow will no longer be able to deform the magnetic field. Such a turning point is defined as the equipartition field strength ($B_T$), at which the magnetic energy density becomes equal to the kinetic energy density of the flow, i.e.,

$$\frac{B_T^2}{\mu_0}=\rho(u'_{rms})^2 \tag{2}$$

where $\mu_0$ is the magnetic permeability. Such a turning point stemming from differential rotation in solar dynamo has a simple replacement in the pulsar magnetosphere, the centrifugal force due to pulsar spin.

As particles in the polar cap of a pulsar are accelerated outwardly by a large unshielded parallel electric field[2], particles of opposite signs are trapped in corotating regions near the equatorial plane[22, 24], which results in an oblique dome–disc particle distribution, with negative particles escaping from both polar caps and positive ones trapped at disc region [25]. Such models would cause a long standing problem that is a charged star surface preventing radiation from possible[26]. Whereas, taking into account of the centrifugal force, such "disc plasma" trapped in closed field lines can be driven toward the light cylinder and eventually contributing to pulsar wind.

As a result, the strength of light cylinder magnetic field is enhanced significantly, which triggers magnetic reconnection at outer magnetosphere region and resulting in pulsar emission. The process of twisting up the last closed field lines and energy relaxation repeat, so that the new last close field takes place of the previous one at the cost of both the rotation energy and magnetic energy of the pulsar.

Such a marginal stable process near the last closed field line or the separatrices can be described by the equation of motion of magnetohydrostatics,

$$\rho\frac{d\mathbf{v}}{dt}=-\nabla p+\mathbf{j}\times\mathbf{B}+\rho\mathbf{g} \tag{3}$$

where the current, $\mathbf{j}=\nabla\times\mathbf{B}/\mu$, can be simplified by $j_y=\frac{1}{\mu}\frac{dB_z}{dx}\approx\frac{2B_z}{\mu\delta}$ (where $\delta$ is the thickness of the current layer) in the Cartesian coordinate as shown in Fig1a.

The centrifugal and gravitational acceleration on a particle, $a=v^2/R$ and $g=GM/R^2$, are balanced at a radius of $R_{eq}^3=GM/\omega^2$. With $R_{lc}=c/\Omega$ denoting the light cylinder radius, the centrifugal force overwhelms the gravity in the case of $R\geq10^{-1}R_{lc}$ for millisecond pulsars; and $R\geq10^{-2}R_{lc}$ for normal pulsars.

As the closed field lines where plasma frozen in are driven towards the light cylinder, Equation (3) is dominated by $\rho v^2/R=|\mathbf{j}\times\mathbf{B}|$. In other words, the centrifugal force is balanced by the magnetic tension near light cylinder,

$$\frac{B^2}{\mu R}=\rho\frac{v^2}{R}\approx\frac{j_y m_e}{ev'}\frac{v^2}{R}\approx\frac{2B}{\mu\delta}\frac{m_e}{ev'}\frac{v^2}{R} \tag{4}$$

where $m_e$ and $e$ are mass and charge of an electron, $v'$ is the speed of charge corresponding to the current $j_y$, paralleling to the thickness direction, $\delta$, of the current layer as shown in Fig1a ($L$ and $b$ are the length and width of the current sheet). The global magnetospheric simulations[14] show two branches of thick Y-shaped current sheet connecting with a thin equatorial sheet where reconnections proceed. By Equation (4), the thickness of the equatorial layer, $\delta$, simply stems from the centrifugal force.

Interestingly, Equation (4) derived from the balance of force yields, $B^2/\mu_0=\rho v^2$, which is equivalent to the balance of energy density occurring in dynamo activity as shown in Equation (2).

The tension of Equation (4) breaks when the velocity in the rest frame of pulsar magnetosphere approaches $v = v_{am} \sim c$, where $v_{am}$ is the plasma speed along the Archimedes line as shown in Fig1a. As a result, Equation (4) can be further simplified by a critical magnetic field,

$$B_T \approx 10^{-3} \frac{v}{v'} \frac{1}{\delta} \approx 10^{-3} \frac{c}{v'} \frac{1}{\delta} \tag{5}$$

In case of a velocity of current flow of $v' \sim 10^3 m/s$, the apex of last closed field lines has a thickness of only $\delta \sim 10^{-2} m$, which corresponds to a magnetic field much greater than that of the light cylinder one, $B_T \gg B_{lc}$, where $B_{lc} = B_s(\frac{R}{R_{lc}})^3$.

While the critical field of, $B_T \sim 10^4$T, is still much weaker than that of the pulsar surface one, $B_s$, so that the strength of the three fields are related by $B_s \gg B_T \gg B_{lc}$. The reconnection of a plasmoid at the critical magnetic field, $B_T \sim 10^4$T, corresponds to an energy density of,

$$\frac{B_T^2}{\mu_0} \approx n_e \gamma m_e c^2, \tag{6}$$

which is sufficient not only producing pairs of energy, $2m_e c^2$, but also accelerating electrons of a number density of $n_e \sim 10^{24} m^{-3}$ to relativistic speed of Lorentz factor, $\gamma \sim 10^2$.

On the other hand, the magnetic diffusion at the critical magnetic field, $B_T$, can invoke a magnetic tension which results in a AW propagating along the field lines, Such a process can be investigated simply by the combination of equation of induction,

$$\frac{\partial \mathbf{B}}{\partial t} = \nabla \times (\mathbf{v} \times \mathbf{B_0}) + \eta \nabla^{\mathbf{2}} \mathbf{B} \tag{7}$$

and equation of motion of Equation (3) simplified as $\rho \frac{d\mathbf{v}}{dt} = \mathbf{j} \times \mathbf{B_0}$, where with the magnetic diffusivity, $\eta$; and $B_0$ is the background magnetic field at the reconnection site satisfying $B_0 \approx B_T$ in a marginal stable state.

Under the usual wave assumption, $exp(-\omega_i t) exp(i\omega_r t)$, a simple dissipation relation is obtained[26],

$$\omega^2 = k^2 v_A^2 - i\omega \frac{k v_A}{R_m}, \tag{8}$$

where $v_A$ is the Alfven speed, and $R_m \equiv L v_A/\eta$ is the magnetic Reynolds number, and $L$ is the length of current sheet at the reconnection site.

The current sheet formed by trapped plasma can be fragmented into a chain of rapidly growing secondary magnetic islands or plasmoids, with the smallest elementary current sheets, of size $\delta$, as shown in Equation (5), so that the equivalent length of current sheet becomes $L \approx \delta$ in Equation (8).

A distribution of such a relativistic particles interact with a distribution of waves leading to the sloshing about of particles in the waves, and resonant wave-particle interactions[26, 27]. Therefore, once a plasmoid gets reconnected at the apex of the last closed fields, the magnetic Reynolds number of Equation (8) becomes $R_m \sim v_A \delta/\eta$, which leads to AW of wave length $\lambda \sim \delta \sim 10^{-2}$m.

Splitting $\omega$ of Equation (8) into a real $\omega_r$ and imaginary $\omega_i$, the wave frequency, $\omega_r \approx k v_A$, corresponds to a time scale of,

$$\tau_r = \frac{2\pi}{\omega_r} \sim 2\pi (\frac{\lambda}{1 \times 10^{-2}})(\frac{3 \times 10^8}{v_A}) \sim 2 \times 10^{-10} s \tag{9}$$

And the damping of such an AW is determined by $\omega_i = -k v_A/(2R_m)$, so that

$$\tau_i = \frac{2\pi}{\omega_i} \sim 2\pi\mu_0 (\frac{\lambda}{1 \times 10^{-2}})^2 (\frac{1}{\eta}) \sim 8 \times 10^{-10} s \tag{10}$$

Consequently, Equation (9) and Equation (10) predict a wave train of length, $s \sim \tau_i c \sim 2 \times 10^{-1}$m, a wave number of, $k \sim 1/\delta \sim 10^2$, and hence, $ks \sim 20 \gg 1$, which corresponds to a GHz nanoburst of short frequency range, $\Delta\omega/\omega = (\omega_r^2 - \omega_i^2)^{1/2}/\omega_r \approx 0.03$, comparable to a typical FRB.

The reconnection determined by Equation (9) and Equation (10) alway takes place at the apex of the last closed field lines which can be achieved by a new last closed field line denoted by (2) catching up the old one (1) as shown in Fig1a.

The duration of a microstructure much shorter than a nanoburst is constrained by both the characteristic frequency of GHz and the coherent condition, $ks \gg 1$. Therefore, the characteristic frequency of GHz, nanoburst, the critical magnetic field, as well as pair production as shown in Equation (5) are closely related in the context of reconnection induced radio emission.

The particles and waves stemming from the magnetic reconnection at the critical field, $B_T$, can undergo resonant wave-particle interaction,

$$\omega - \mathbf{k} \cdot \mathbf{v} = \mathbf{0}, \tag{11}$$

in an unmagnetized plasma.

The feedback between the AW field and particle bunching resulting in a unison growth of them, which is equivalent to a reactive instability expected in models of coherent emission.

## III. CCE

The bunch in phase with AW leads to a CCE. The energy radiated per unit solid angle per unit frequency interval from a bunch with volume $V$ and number of $N_e \sim n_e V$ particles drifting along a curved field line[28],

$$\frac{dI_{tot}}{d\omega d\Omega} = \frac{dI}{d\omega d\Omega} F_\omega(N_e) \tag{12}$$

where $F_\omega(N_e)$ is a dimensionless parameter denoting the enhancement factor due to coherence defined,

$$F_\omega(N) = |\Sigma_j^N e^{-i\omega(\mathbf{n} \cdot \Delta \mathbf{r}_j/c)}|^2 \tag{13}$$

where, $\mathbf{n}$, is the unit vector to the observer, and $\Delta\mathbf{r}_j$ is a section of the bunch length $L_{bc}$. The emission of such a bunch could be coherent only if all such small sections are in phase, with each small section of size $\Delta r_j \ll \lambda$. Such a phase relationship required in small sections of a bunch is difficult to achieve in the usual bunch models.

While the reconnection induced pairs and AW, with resonant wave-particle interactions automatically gives rise a coherent bunch responsible for coherent emission. Because it allows the growth or damping of wave, and the scattering and acceleration of particles, so that the particle sees the electric field of wave as static fielding its rest frame[26].

As a result, an AW of wave length, $\lambda \sim 1\times10^{-2}$m, and a coherent length $c\tau_i \sim 20\lambda$ corresponds to a coherent bunch of length comparable to that of the wave train, $L_{bc} \sim \sum \Delta r_j \sim 20\lambda$. Then simply applying the half wave superposition, the enhancement factor of such an in phased bunch becomes $F_\omega(N_e) = N_e^2$, responsible for the emission of a coherent nanoburst.

The fast reconnection of a plasmoid occurring at the apex of the last closed field line produces a nanoburst as shown in Fig1a. Such a process is replaced by a new last closed field lines and a new nanoburst... The swing of those nanobursts through a pulse window results in the single pulse of a pulsar, with an enhancement factor of Equation (13) of,

$$F_\omega(N_e, N) = NN_e^2 \tag{14}$$

where $N_e$ and $N$ are number of particles in a nanoburst and number of nanoshots in a single pulse respectively. This explains why the single pulse of a pulsar appears much dimmer than a nanoburst.

This provide a concrete mechanism to the speculation[21] that: microbursts are incoherent superpositions of short-lived narrowband, nanoshots, and all microbursts are clumps of nanoshots. In such a case, the broadband of each such microburst can be interpreted by widening the frequency range of the centre frequencies of the nanoshots (each with a very short frequency range as shown under Equation (10)) in a microburst[21].

Twisting magnetic field to the critical level, $B_T$, near the light cylinder can invoke rapid magnetic reconnection well accounting for coherency, microstructure, characteristic frequency of GHz of radio emission of pulsars.

To allow the AW propagate through plamoids, the plasma frequency must be lower than that of the characteristic frequency of 1GHz,

$$\omega_p = (\frac{4\pi n_e e^2}{m_e})^{1/2} \lesssim \omega_A \sim 1GHz. \tag{15}$$

which in turn demands, $n_e \lesssim 3\times10^{24}m^{-3}$. Notice the plasma frequency above is much greater than the cyclotron frequency, $\omega_p \gg \omega_{cy} \approx eB_T/(m_e c) \approx 10^7$Hz. Substituting such a limit on particle density into the constraint of Equation (6), the Lorentz factor is required to be $\gamma \gtrsim 3\times10^2$. In other words, the energy dissipation through reconnection at the critical magnetic field, $B_T$, can both produce and accelerate pairs of number density of $n_e \lesssim 3\times10^{24}m^{-3}$ to relativistic speed of Lorentz factor, $\gamma \gtrsim 3\times10^2$, which form a coherent bunch and resulting in coherent curvature emission through subsequent interaction with the flux tube formed by open field lines.

Pairs ejected from the reconnection site drift along a flux tube formed by open field lines as shown in Fig1 at speed $v_{am} \sim c$ in the rest frame of the pulsar magnetosphere, such relativistic plasma can give rise to curvature radiation of effective frequency of

$$\nu = \frac{\gamma^3 c}{\rho} \sim 1GHz \tag{16}$$

which corresponds to a power of coherent curvature radiation[29] ,

$$P_{cv} = \frac{N_e^2 e^2 c\gamma^4}{\rho^2} \tag{17}$$

where $N_e = n_e V$ is the number of charged particles contained in a bunch of volume, $V$. It worth mention that the velocity of the emission site is $v \approx v_{am} - \Omega R_{lc} \approx 0$ in the laboratory frame.

The interacting of the coherent bunch of length, $L_{ch} \sim 20\lambda$ with open magnetic field line of curvature radius, $\rho \sim R_{lc}$, corresponds to a spread angle of, $\theta \sim L_{ch}/R_{lc} \sim 10^{-8}$, the misalignment angle between the front and end of a bunch emitting radio waves tangentially to the field lines, which is much less than the angle of emission cone, $1/\gamma \sim 10^{-2}$ with $\gamma \sim 100$ denoting the Lorentz factor of plasma. Consequently, the coherency of each nanoburst is ensured, while different nanobursts can be incoherent as they swing through the line of sight.

Moreover, bunch models suffer from other problems like: the growth of the instability is not fast enough; and velocity dispersion resulted random-phase rather than phase coherent ones[27]. Again the new scenario provides both fast instability and limited velocity dispersion. Because the balance between the centrifugal force and the magnetic tension breaks at the critical magnetic field, $B_T$, the resultant magnetic reconnection is triggered at the apex of last closed field lines with a layer thickness, $\delta \sim 10^{-2}$m, corresponding to a fast instability of frequency of GHz. Furthermore, such a AW with has very limited frequency dispersion as shown in Equation (9) and Equation (10), and hence limited velocity dispersion under the resonant particle-wave interaction. Therefore, the problems of coherent emission by bunch can be solved in the new scenario.

On the other hand, as the reconnection always takes place at the apex of last closed field line, the subsequent radiation should propagate in the flux tube of open field lines with much lower particle density than that inside the current layer. Such a "density cavity" like environment deviates from models of reconnection by coalescence of magnetic islands in the current sheet, where

magnetic perturbations should propagate in the dense current sheet[18].

## IV. CIRCUIT AND OPM

At the reconnection site, both the outflow and inward beams are accelerated by the reconnection electrical field near X line. The presence of guided field in the X line region of the reconnection site leads to strongly field aligned distribution of beams of electron and positron[30]. One pair of electron and positron return to the pulsar surface directly along separatrices of the X line, as shown in Fig1b. And the other pair of energetic electron and positron beams move along opposite pair of separatrices of the X line away from the reconnection site, giving rise to coherent radiation and eventually contributing to the pulsar wind.

The internal electric field causes a structure of dome-disc charge in which particles of the same sign escape from both polar caps, and particles of opposite signs are trapped in corotating regions near the equatorial plane[22, 24], as shown at bottom of Fig1b. In the new scenario, the trapped disc charge is driven toward the equatorial sheet by centrifugal force which triggers magnetic reconnection and generates pair production. The resultant return plasma drifting along the separatrices to the pulsar surface as shown in bottom of Fig1b.

As shown at bottom right of Fig1b, one beam of return positrons would be neutralized by the negative charge at dome. In contrast, the other beam of return electrons as shown in bottom left of Fig1b, would provide extra negative charges at this pole which would distributed evenly two domes by the internal electric field of the star[22, 24] as shown at bottom right of Fig1b, so that the original structure of dome-disc charge can be resumed.

The charge neutrality of the pulsar is ensured, as long as (1) the loss of negative charge at domes toward the pulsar wind is equivalent to the positive disc charge driven to the reconnection site; and (2) the return electrons and positrons are approximately charge neutral. This automatically results in a marginal stable circuit of the pulsar magnetosphere.

In contrast, charge neutrality has been a problem in the case of disc charges trapped in the configuration of dome-disc charge[22, 24].

The circuit stemming from dynamo process in magnetosphere is compatible with numerical simulations which exhibit that pair production can be triggered in the diffusing region, where half return to the pulsar surface along separatrices, and other half plasma eject out contributing to the pulsar wind[31].

One of the most fascinating features of pulsar radiation is the occurrence of OPM, i.e., the two electromagnetic waves with orthogonal electric vectors. The origin of OPM is still an open question.

As proposed by Gangadhara[32] OPM can be produced by the relativistic positrons and electrons drifting along a curved magnetic field line, during which an electron and a positron would experience the centrifugal force $F_C$ of identical direction; and the magnetic Lorentz force $F_B$ of opposite direction. As a result, the sum of the two forces, $F_C+F_B$, on a positron is approximately perpendicular to that of an electron under the assumption of $|F_c| \approx |F_B|$ in magnitude.

Differing from the OPM occurring by electrons and positron at the same curved field line[32], the configuration of the new scenario as shown in Fig1b corresponds to a separated electrons and positrons on opposite polarity of magnetic field lines, which results in opposite senses of gyration. As shown in Fig1b, magnetic Lorentz force $F_B$ of electrons and positrons are at opposite direction, combined with the centrifugal (inertial) force $F_C$ of same direction, the total force on an electron is approximately perpendicular to that of a position, $F_b \perp F_e$ corresponding to an orthogonal electric vectors, in the case of $|F_c| \approx |F_B|$. Therefore, OPM is achieved naturally, which can account for the polarization states like PSR J0953+0755.

The dynamo process in pulsar magnetosphere corresponding energy relaxation not only produces pairs but also accelerate them into relativistic speed, which naturally accounts for coherency, microstructure, characteristic frequency, density cavity, polarization, OPM, and circuit required in radio emission of pulsars.

## V. GLOBAL-LOCAL INTERACTION AND IMPLICATION TO PULSARS AND FRBS

As shown in Section (II), folding up magnetic field to the critical amplitude of $B_T \sim 10^4$T triggers magnetic reconnection resulting in subsequent coherent emission. This section further discusses the energy budget and resultant intermittency, as well as frequency-width relation and trombone on various pulsars and FRBs.

### A. The Crab pulsar and PSR J0437-4715

For young pulsars, i.e., Crab pulsar with spin period $P = 33ms$, the surface and light-cylinder magnetic field are, $B_s \approx 4 \times 10^8$T and $B_{lc} \approx 1 \times 10^2$T respectively. Therefore, a number of pulsar spins of $N \approx 30$ can wind up the magnetic field to the critical value, $B_T \sim 10^4$T, corresponding to a magnetic energy of $E_H = B_T^2 V_Y/\mu$, where $V_Y \sim L_\delta L_b L_Y$.

In the case of a current sheet length of $L_Y \sim 10^{-2} R_{lc} \sim 10^4$m, width $L_b \sim 10^{-2} L_Y \sim 10^2$m, and thickness, $L_\delta \sim 10^{-2} L_Y \sim 10^2$m, the magnetic energy pile up in 30 pulsar spins is read,

$$E_H \sim 10^6 (\frac{N_s}{30})^2 (\frac{B_{lc}}{10^2})^2 (\frac{L_\delta}{10^2})(\frac{L_b}{10^2})(\frac{L_Y}{10^4}) \sim 10^{22} J \quad (18)$$

Transfer such an energy of global field into the reconnection site at the apex of last closed field lines, plasma

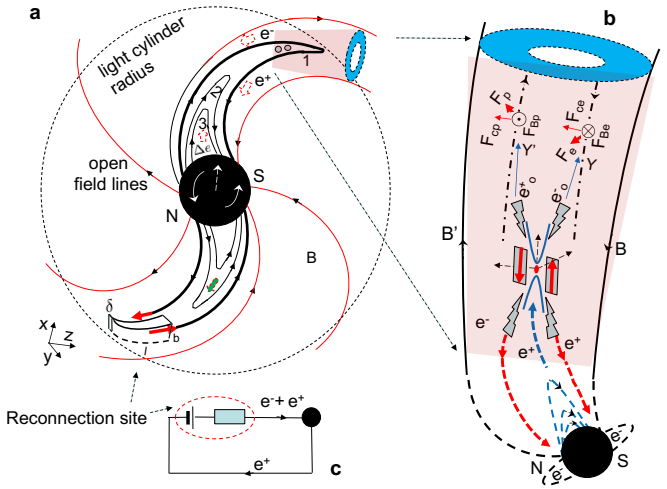


FIG. 1. A schematic configuration of the dynamo magnetosphere. Panel a: pulsar spin deformed last closed field lines surrounded by flux tube of open field lines. Small circles denote plasmoids inside the upper last closed field line, their reconnection gives rise to beams and waves. The geometry of current sheet at reconnection site is shown at bottom of the spiral. Panel b: reconnection site with guided field which separates the electron and positron beams. The outward beams interact with the open field lines invoking coherent emission with an OPM polarity denoted by perpendicular direction of force on a positron $F_p$, and an electron, $F_e$. And the return beams contribute to the surface charge. Panel c: the return electron and positrons together with the dome-disc charge form a closure circuit.

beams flow from the Y-shaped layer of volume, $V_Y$ into reconnection region of volume, $V_{rec} \sim \delta bl$, which corresponds to a suppression of current layer of Sweet-Parker satisfying mass conservation,

$$v_x L_\delta \approx v_z \delta$$

Accordingly, magnetic Reynolds changes from $R_m \sim v_A L_Y/\eta$ at Y-shaped current sheet to $R_m \sim v_A \delta/\eta$ at the apex of last closed field line, triggering a fast plasmoid reconnection, with power read, $P_R = \frac{B_T^2}{\mu}\delta b v_z$, which can be rewritten as

$$P_R \sim 10^6 (\frac{N_s}{30})^2 (\frac{B_{lc}}{10^2})^2 (\frac{\delta}{10^{-2}})(\frac{b}{10^2})(\frac{v_z}{10^8}) \sim 10^{22} W \quad (19)$$

where $v_z \sim c$ is the drifting speed of plasma at the dissipation region observed at the rest frame of the spinning pulsar. While in the laboratory frame such a drifting velocity becomes, $v \approx v_z - \Omega R_{lc} \approx 0$. In fact, the energy relaxation of Equation (19) is similar to ballooning instability occurring in the near-Earth plasma sheet resulting in substorm expansion[33], which is supported by laboratory experiment[34].

The oscillation of pile up and relaxation of magnetic energy of Equation (18) and Equation (19) can be estimated as,

$$\dot{E}_H \approx \frac{E_H}{N_s P} \approx P_R, \quad (20)$$

For some pulsars, like the Crab pulsar the times scale of such an oscillation can be accomplished in a second, $N_s P \sim 1$s.

In fact, the radiation power of Equation (19) is compatible with radio emission of the Crab pulsar[35], which corresponds to a very small fraction (typically $10^{-6}$ to $10^{-5}$) of the total energy loss.

The relativistic pairs ejected from the reconnection site drift along the flux tube formed the open field lines invoking curvature radiation, with a curvature radius of $\rho \sim R_{lc}$. Together with the frequency constraint of Equation (16), the Lorentz factor of $\gamma \sim 300$ and number density of charged particles, $n_e \sim 3 \times 10^{24} m^{-3}$ can be estimated.

The reconnection of a plasmoid proceeds in a small volume of $V_{rec} \sim \delta bl \sim 1m^3$ at the apex of the last closed field line, giving rise to a power of coherent curvature radiation, $P_{cv} \sim 10^{17}$W by Equation (17). Furthermore, to consist with observational power of radio emission of the Crab pulsar[35], $P_{ob} \sim 10^{22}$W, a number of plasmoids of $N \sim 10^5$ need to be reconnected per second. Such a coherent curvature emission provides a sample of coherent emission as shown in Equation (14), in which the number of plasmoids and number of plasma in a plasmoid are concretely, $N \sim 10^5$ and $N_e \sim 10^{24} m^{-3}$, respectively.

The millisecond pulsar, PSR J0437-4715 (spin period $P \approx 5.8ms$), corresponds to a surface magnetic field of only $B_s \approx 6 \times 10^4$T, which is 4 order of magnitude less than that of the Crab pulsar. While simply change the pile up spins number to, $N_s \sim 5 \times 10^2$ (also satisfying $N_s P \approx 1$s), its pile up energy, power of curvature radiation and energy budget of Equation (18)-Equation (20) are almost identical that of the Crab pulsar.

Consequently, similarities between the Crab pulsar and millisecond pulsars in radio emission which is difficult to understand in the context of polar cap models as well as magnetic reconnection at light cylinder magnetic, $B_{lc}$ can be well interpreted by the dynamo process.

### B. PSR J0953+0755, frequency-width relation and PSR J0901-4046, the death line problem

PSR J0953+0755 is a bright nonrecycled pulsar whose single-pulse fluence variability is reportedly large[36] . With period of $P \approx 0.253$s, a spindown age of $1.75 \times 10^7$yr, the surface and light curve magnetic fields of this pulsar are $B_s \approx 2 \times 10^7$T and $B_{lc} \approx 1 \times 10^{-2}$T respectively. To achieve the critical magnetic field, $B_T \sim 10^4$T, a pile up time scale of $\tau \sim N_s P \sim 10^5$s with $N_s \sim 10^6$ pulsar spins are required. In the case of a Y-shaped current sheet length, $L_Y \sim 10^{-2} R_{lc} \sim 1 \times 10^7$m, width $L_b \sim 10^{-3} L_Y$, and thickness, $L_\delta \sim 10^{-4} L_Y$, the folding

up magnetic energy is of $E_H \sim 10^{24}$J by substitution above parameters into Equation (18).

Such a magnetic energy piled up of PSR J0953+0755 can radiate at the observational power of radio emission[35], $P_{rd} \sim 10^{19}$W, for a time interval of $E_H/P_{sd} \sim 10^5$s. Furthermore, with curvature radius $\rho \sim R_{lc} \sim 1 \times 10^9$m, the constraint of Equation (16), requires a Lorentz factor of $\gamma \sim 900$ and a number density of charged particles, $n_e \sim 1 \times 10^{24} m^{-3}$, which corresponds to a power of curvature radiation of PSR J0953+0755, $P_{cv} \sim 5 \times 10^{12}$W. Therefore, in an pulse window of PSR J0953+0755 , it required to reconnect a number $N \sim 10^5$ plasmoids.

The nanoshots as shown in Equation (9) and Equation (10), reproduce AWs of GHz and beams in phase with the AWs. Such origin beams and AWs radiate and give rise to GHz emission while drifting along the flux tube formed by open field lines becoming wider and wider down stream.

On the other hand, such GHz radiation scattered by plasma leftover by previous activities in the flux tube, resulting in two effects. Firstly, the GHz radiation transfers energy into the plasma invoking lower frequency emission at i.e., $10^1 - 10^2$MHz; secondly the GHz photons gain energy from relativistic plasma, resulting in $10^1 - 10^2$GHz radiation.

This explains the frequency-width relation of the Crab pulsar, which shows a narrower and sharper pulse profile at 1.4GHz, while wider and more diffused profile at both lower frequencies, $10^2$MHz; and higher frequencies, 4.7GHz[37]. In comparison, the width of pulse profiled of PSR J0953+0755 at 1.4GHz emission is roughly half of the 55MHz one[36], implying that only the first effect can work in the slow plasma of this normal pulsar, but not sufficient for the second one. As such low frequency radiation locates downstream closer to the Earth which arrives earlier, so that appearance of sad trombones in PSR J0953+0755 and the repeating FRB 20180916B [36] can be automatically interpreted. Correspondingly, both sad and happy trombones should occur in the Crab pulsar [37].

PSR J0901-4046 locates beyond the "death line"[2, 17], and exhibits quasi-periodicity and partial nulling[38]. Simply replacing the pile up time by $\tau \sim N_s P \sim 10^{11}$s, its balance of energy budget and radiation properties resemble those of PSR J0953+0755 also exhibiting partial nulling[39].

### C. Nonlinearity

The dissipation of Equation (20) does not alway proceed in marginal stable state with normal emission, i.e., on some days PSR J0953+0755 exhibits a large number of giant pulses, there are other days when it enters nulling state with no detectable emission in the power spectrum or in the folded pulse data[39].

Interestingly, one of RRAT, neutron stars emitting sporadic radio bursts, RRAT J1913+1330, displays sequential pulse trains during active phases with significant pulse variations in profile, fluence, flux, and width, as well as between adjacent sequential pulses[40].

And repeat FRB 121102 exhibits 1,652 independent bursts with a peak burst rate of 122 per hour, in 59.5 hours spanning 47 days [41].

Such striking similarities indicate that normal pulsars, nulling pulsars, and FRBs share common mechanism, the nonlinearity occurring the dynamo process of the pulsar magnetosphere provides a simple and natural candidate. In fact, the nonlinearity in the interaction between global magnetic energy and local dissipation has been studied extensively in astronomical objects.

A convenient approach is to investigate helicity density transport near the marginal state. When adding a small perturbation to the current sheet in the marginal state, the local current gradient will exceed the critical value, which leads to current sheet fragmentation or plasmoid formation[16, 42]. The evolution equation for magnetic helicity density is essentially based on the induction equation of Equation (7), which takes the form of the Burgers equation[43]. In such a case, helicity density transport near the marginal state is intermittent and episodic. And some detailed analysis[16] shows that there are indeed soliton-like solutions.

The energy conservation as shown in Equation (20), can be simplified by energy accumulation of number $N_s$ pulsar spins dissipating into giant pulses of number of, $N_s N$, with fluence of giant pulse of $E_G$.

$$N_s(t)N(t)E_G(t) \approx C(t) \tag{21}$$

The marginal stable state corresponds to averaged values of Equation (21), i.e., for Crab pulsar, $N_s(t) \sim 30$, $N(t) \sim 10^5$, and $E_G(t) \sim 10^{40}$K. In contrast, deviation from marginal state corresponds to time varying values of Equation (21) determined by nonlinearity of Equation (7), such that much brighter giant pulse, with fluence $E_G \gg 10^{40}$K resembling FRBs, can be achieved by different combination of parameters of Equation (21).

Likewise, normal pulsars and old pulsars, can either emit intermittent and episodic giant pulses mimicing RRATs; or much stronger giant pulses of fluence $E_G \gg 10^{40}$K responsible for FRBs at the cost of much larger pile up spins, $N_s(t)$ than that of young pulsars, which provides an explanation to the repeating FRB 20200120E found in an M81 globular cluster[44].

In summary the dynamo process in pulsar magnetosphere can interpret coherent curvature radiation and intermittency of pulsars. Through centrifugal force the magnetic field can be amplified to the critical value, $B_T \sim 10^4$T, which results in local dissipation (the magnetic reconnection) responsible for: theoretical problems, (1) pair production, (2) nanoshots, (3) CCE, (4) circuit closure, (5) density cavity; and observational problems, (a) character frequency of GHz, (b) correlation of frequency-pulse width and trombone, (c) OPM polarization, (d) intermittency of pulsars and FRBs, (e) death

line problem.

Interestingly, phenomena (a-d) exhibited in PSR J0953+0755 can be explained together by the dynamo scenario. Many aspects of the new scenario await further investigation and observational test.




[1] P. A. Sturrock, A Model of Pulsars, Astrophys. J. **164**, 529 (1971).

[2] M. A. Ruderman and P. G. Sutherland, Theory of pulsars: polar gaps, sparks, and coherent microwave radiation., Astrophys. J. **196**, 51 (1975).

[3] G. Benford and R. Buschauer, Coherent pulsar radio radiation by antenna mechanisms: general theory., Monthly Notices of the Royal Astronomical Society **179**, 189 (1977).

[4] J. Gil, Y. Lyubarsky, and G. I. Melikidze, Curvature Radiation in Pulsar Magnetospheric Plasma, Astrophys. J. **600**, 872 (2004), arXiv:astro-ph/0310621 [astro-ph].

[5] D. B. Melrose, M. Z. Rafat, and A. Mastrano, Pulsar radio emission mechanisms: a critique, Monthly Notices of the Royal Astronomical Society **500**, 4530 (2021), arXiv:2006.15243 [astro-ph.HE].

[6] I. Contopoulos, D. Kazanas, and C. Fendt, The Axisymmetric Pulsar Magnetosphere, Astrophys. J. **511**, 351 (1999), arXiv:astro-ph/9903049 [astro-ph].

[7] A. Spitkovsky, Three-dimensional Pulsar Magnetosphere, in *AAS/High Energy Astrophysics Division #9*, AAS/High Energy Astrophysics Division, Vol. 9 (2006) p. 4.03.

[8] K. Parfrey, A. M. Beloborodov, and L. Hui, Twisting, Reconnecting Magnetospheres and Magnetar Spindown, **754**, L12 (2012), arXiv:1201.3635 [astro-ph.HE].

[9] D. A. Uzdensky and A. Spitkovsky, Physical Conditions in the Reconnection Layer in Pulsar Magnetospheres, Astrophys. J. **780**, 3 (2014), arXiv:1210.3346 [astro-ph.HE].

[10] I. Contopoulos, D. Kazanas, and C. Fendt, The Axisymmetric Pulsar Magnetosphere, Astrophys. J. **511**, 351 (1999), arXiv:astro-ph/9903049 [astro-ph].

[11] X.-N. Bai and A. Spitkovsky, Modeling of Gamma-ray Pulsar Light Curves Using the Force-free Magnetic Field, Astrophys. J. **715**, 1282 (2010), arXiv:0910.5741 [astro-ph.HE].

[12] A. A. Philippov and A. Spitkovsky, Ab Initio Pulsar Magnetosphere: Three-dimensional Particle-in-cell Simulations of Axisymmetric Pulsars, **785**, L33 (2014), arXiv:1312.4970 [astro-ph.HE].

[13] A. Y. Chen and A. M. Beloborodov, Electrodynamics of Axisymmetric Pulsar Magnetosphere with Electron-Positron Discharge: A Numerical Experiment, **795**, L22 (2014), arXiv:1406.7834 [astro-ph.HE].

[14] A. Philippov, D. A. Uzdensky, A. Spitkovsky, and B. Cerutti, Pulsar Radio Emission Mechanism: Radio Nanoshots as a Low-frequency Afterglow of Relativistic Magnetic Reconnection, **876**, L6 (2019), arXiv:1902.07730 [astro-ph.HE].

[15] L. Woltjer, A Theorem on Force-Free Magnetic Fields, Proceedings of the National Academy of Science **44**, 489 (1958).

[16] P. H. Diamond and M. Malkov, Dynamics of helicity transport and Taylor relaxation, Physics of Plasmas **10**, 2322 (2003).

[17] K. Chen and M. Ruderman, Pulsar Death Lines and Death Valley, Astrophys. J. **402**, 264 (1993).

[18] Y. Lyubarsky, Radio emission of the Crab and Crab-like pulsars, Monthly Notices of the Royal Astronomical Society **483**, 1731 (2019), arXiv:1811.11122 [astro-ph.HE].

[19] D. Melrose, Pulse Emission Mechanisms, in *Young Neutron Stars and Their Environments*, Vol. 218, edited by F. Camilo and B. M. Gaensler (2004) p. 349, arXiv:astro-ph/0308471 [astro-ph].

[20] J. H. Crossley, J. A. Eilek, T. H. Hankins, and J. S. Kern, Short-lived Radio Bursts from the Crab Pulsar, Astrophys. J. **722**, 1908 (2010), arXiv:1009.0735 [astro-ph.HE].

[21] J. A. Eilek and T. H. Hankins, Radio emission physics in the Crab pulsar, Journal of Plasma Physics **82**, 635820302 (2016), arXiv:1604.02472 [astro-ph.HE].

[22] F. C. Michel and H. Li, Electrodynamics of neutron stars, Physics Reports **318**, 227 (1999).

[23] W. M. Elsasser, Hydromagnetic Dynamo Theory, Reviews of Modern Physics **28**, 135 (1956).

[24] E. A. Jackson, A new pulsar atmospheric model. I. Aligned magnetic and rotational axes., Astrophys. J. **206**, 831 (1976).

[25] A. Spitkovsky, Electrodynamics of Pulsar Magnetospheres, in *Young Neutron Stars and Their Environments*, Vol. 218, edited by F. Camilo and B. M. Gaensler (2004) p. 357, arXiv:astro-ph/0310731 [astro-ph].

[26] *Saas-Fee Advanced Course 24: Plasma Astrophysics* (1994).

[27] D. B. Melrose, Maser pulse emission mechanisms, in *Pulsars: 13 Years of Research on Neutron Stars*, Vol. 95, edited by W. Sieber and R. Wielebinski (1981) pp. 133–139.

[28] Y.-P. Yang and B. Zhang, Bunching Coherent Curvature Radiation in Three-dimensional Magnetic Field Geometry: Application to Pulsars and Fast Radio Bursts, Astrophys. J. **868**, 31 (2018), arXiv:1712.02702 [astro-ph.HE].

[29] A. J. Cooper and R. A. M. J. Wijers, Coherent curvature radiation: maximum luminosity and high-energy emission, Monthly Notices of the Royal Astronomical Society **508**, L32 (2021), arXiv:2108.07818 [astro-ph.HE].

[30] P. L. Pritchett, Relativistic electron production during guide field magnetic reconnection, Journal of Geophysical Research (Space Physics) **111**, A10212 (2006).

[31] I. Contopoulos, J. Pétri, and P. Stefanou, Hybrid numerical simulations of pulsar magnetospheres, Monthly Notices of the Royal Astronomical Society **491**, 5579 (2020), arXiv:1909.13504 [astro-ph.HE].

[32] R. T. Gangadhara, Emission in spin-powered pulsars and polarization position angle., **314**, 853 (1996).

[33] P. Zhu and J. Raeder, Ballooning instability-induced plasmoid formation in near-Earth plasma sheet, Journal of Geophysical Research (Space Physics) **119**, 131 (2014).

[34] Y. Kuramitsu, T. Moritaka, Y. Sakawa, T. Morita, T. Sano, M. Koenig, C. D. Gregory, N. Woolsey, K. Tomita, H. Takabe, Y. L. Liu, S. H. Chen, S. Matsukiyo, and M. Hoshino, Magnetic reconnection driven

by electron dynamics, Nature Communications **9**, 5109 (2018).

[35] G. I. Melikidze, J. A. Gil, and A. D. Pataraya, The Spark-associated Soliton Model for Pulsar Radio Emission, Astrophys. J. **544**, 1081 (2000), arXiv:astro-ph/0002458 [astro-ph].

[36] A. V. Bilous, J. M. Grießmeier, T. Pennucci, Z. Wu, L. Bondonneau, V. Kondratiev, J. van Leeuwen, Y. Maan, L. Connor, L. C. Oostrum, E. Petroff, J. P. W. Verbiest, D. Vohl, J. W. McKee, G. Shaifullah, G. Theureau, O. M. Ulyanov, B. Cecconi, A. H. Coolen, S. Corbel, S. Damstra, H. Dénes, J. N. Girard, B. Hut, M. Ivashina, O. O. Konovalenko, A. Kutkin, G. M. Loose, H. Mulder, M. Ruiter, R. Smits, P. L. Tokarsky, N. J. Vermaas, V. V. Zakharenko, P. Zarka, and J. Ziemke, Dual-frequency single-pulse study of PSR B0950+08, **658**, A143 (2022), arXiv:2109.08500 [astro-ph.HE].

[37] T. H. Hankins and J. A. Eilek, Radio Emission Signatures in the Crab Pulsar, Astrophys. J. **670**, 693 (2007), arXiv:0708.2505 [astro-ph].

[38] M. Caleb, I. Heywood, K. Rajwade, M. Malenta, B. W. Stappers, E. Barr, W. Chen, V. Morello, S. Sanidas, J. van den Eijnden, M. Kramer, D. Buckley, J. Brink, S. E. Motta, P. Woudt, P. Weltevrede, F. Jankowski, M. Surnis, S. Buchner, M. C. Bezuidenhout, L. N. Driessen, and R. Fender, Discovery of a radio-emitting neutron star with an ultra-long spin period of 76 s, Nature Astronomy **6**, 828 (2022), arXiv:2206.01346 [astro-ph.HE].

[39] A. K. Singal and H. O. Vats, Giant-pulse Emission from PSR B0950+08, **144**, 155 (2012), arXiv:1209.5093 [astro-ph.HE].

[40] S. B. Zhang, J. J. Geng, J. S. Wang, X. Yang, J. Kaczmarek, Z. F. Tang, S. Johnston, G. Hobbs, R. Manchester, X. F. Wu, P. Jiang, Y. F. Huang, Y. C. Zou, Z. G. Dai, B. Zhang, D. Li, Y. P. Yang, S. Dai, C. M. Chang, Z. C. Pan, J. G. Lu, J. J. Wei, Y. Li, Q. W. Wu, L. Qian, P. Wang, S. Q. Wang, Y. Feng, and L. Staveley-Smith, RRAT J1913+1330: an extremely variable and puzzling pulsar, arXiv e-prints , arXiv:2306.02855 (2023), arXiv:2306.02855 [astro-ph.HE].

[41] D. Li, P. Wang, W. W. Zhu, B. Zhang, X. X. Zhang, R. Duan, Y. K. Zhang, Y. Feng, N. Y. Tang, S. Chatterjee, J. M. Cordes, M. Cruces, S. Dai, V. Gajjar, G. Hobbs, C. Jin, M. Kramer, D. R. Lorimer, C. C. Miao, C. H. Niu, J. R. Niu, Z. C. Pan, L. Qian, L. Spitler, D. Werthimer, G. Q. Zhang, F. Y. Wang, X. Y. Xie, Y. L. Yue, L. Zhang, Q. J. Zhi, and Y. Zhu, A bimodal burst energy distribution of a repeating fast radio burst source, Nature (London) **598**, 267 (2021), arXiv:2107.08205 [astro-ph.HE].

[42] Z. B. Guo, P. H. Diamond, and X. G. Wang, Magnetic Reconnection, Helicity Dynamics, and Hyper-diffusion, Astrophys. J. **757**, 173 (2012).

[43] Z. B. Guo, P. H. Diamond, and X. G. Wang, Magnetic Reconnection, Helicity Dynamics, and Hyper-diffusion, Astrophys. J. **757**, 173 (2012).

[44] K. Nimmo, J. W. T. Hessels, M. P. Snelders, R. Karuppusamy, D. M. Hewitt, F. Kirsten, B. Marcote, U. Bach, A. Bansod, E. D. Barr, J. Behrend, V. Bezrukovs, S. Buttaccio, R. Feiler, M. P. Gawroński, M. Lindqvist, A. Orbidans, W. Puchalska, N. Wang, T. Winchen, P. Wolak, J. Wu, and J. Yuan, A burst storm from the repeating FRB 20200120E in an M81 globular cluster, Monthly Notices of the Royal Astronomical Society **520**, 2281 (2023), arXiv:2206.03759 [astro-ph.HE].